

K. Billon¹

University of Lyon,
Lyon Central School,
LTDS UMR 5513,
F-69134 Ecully, France
e-mail: kevin.billon@ec-lyon.fr

G. Zhao

MOE Key Laboratory of TianQin Mission,
TianQin Research Center for Gravitational Physics
and School of Physics and Astronomy,
Frontiers Science Center for TianQin,
CNSA Research Center for Gravitational Waves,
Sun Yat-Sen University,
Zhuhai 519082, China
e-mail: zhaoguoying@mail.sysu.edu.cn

C. Collette

University of Liège,
Precision Mechatronics Laboratory,
Department of Aerospace and
Mechanical Engineering,
9, allée de la découverte,
4000 Liège, Belgium
Free University of Brussels,
Department of BEAMS,
50, F.D. Roosevelt Avenue,
1050 Brussels, Belgium
e-mail: christophe.collette@ulb.be

S. Chesné

University of Lyon, INSA-Lyon,
CNRS UMR5259, LaMCoS,
F-69621, France
e-mail: simon.chesne@insa-lyon.fr

Hybrid Mass Damper: Theoretical and Experimental Power Flow Analysis

In this paper, a hybrid mass damper (HMD) and its hyperstability due to a power flow approach are studied. The HMD proposed combines an active control system with an optimal passive device. The initial passive system is an electromagnetic tuned mass damper (TMD) and the control law is a modified velocity feedback with a phase compensator. The resulting hybrid controller system is theoretically hyperstable and ensures fail-safe behavior. Experiments are performed to validate the numerical simulation and provide good results in terms of vibration attenuations. Both excitation from the bottom in the frequency domain and shock response in the time domain are tested and analyzed. The different power flows in terms of active and reactive powers are estimated numerically and experimentally on the inertial damper (passive and active) and on the HMD. Moreover, through a mechanical analogy of the proposed system, it is shown that this hybrid device can be seen as an active realization of an inerter based tuned-mass-damper associated with a sky-hook damper. Observations and analysis provide insight into the hyperstable behavior imposed by the specific control law. [DOI: 10.1115/1.4053480]

Keywords: active vibration, dynamics, noise control, smart materials and structures

1 Introduction

Tuned mass dampers (TMD) and dynamic vibration absorbers (DVA) exhibit interesting properties in terms of vibration attenuation. They are passive devices which are widely used in industrial sectors like aerospace and civil engineering [1–5]. The performances of these practical and robust devices are directly linked to the mass ratio between the weight of the absorber and that of the vibrating primary structure. The natural frequency of the TMD is tuned to a frequency near the natural frequency of the primary structure, and the vibration energy is dissipated through the damping in the TMD. The most popular tuning method is called equal peak design [6] with improvements for non-linear systems [7,8] and the integration of robust design [9]. The main disadvantage of a TMD is the sensitivity of the tuned frequency, its optimal damping ratio and the resulting difficulties of tuning these mechanical systems. Other passive systems exist such as the electromechanical shunted damper [10–12], the shunted piezoelectric patch [13,14], and the particle tuned mass damper [15].

A more efficient method is to use active mass dampers (AMD) proposed by Ref. [16]. The performance obtained is better than those of passive systems but active systems are generally more complex and costly. A compromise must be found between

performance and cost. Nevertheless, active control requires sensors (strain, displacement, velocity, acceleration, force) and actuators (force, inertia). The communication between actuators and sensors is directly linked to the design of the controller (feedback or feedforward), without neglecting robustness and stability. In order to control a lightly damped structure, the active damping feedback control strategy is often used. Active damping can reduce the response amplitude of the structure around its resonance frequencies. A model of the structure is not needed and stability is guaranteed by a co-located pair consisting of an actuator and a sensor. In the literature, active damping strategies can be found such as the lead controller that produces a phase lead, hence its name, direct velocity feedback (DVF) which can be considered as a particular case of lead controller (the actuator is driven with a signal proportional to the velocity, which is a natural way to add damping), positive position feedback (PPF) proposed by Refs. [17,18], integral force feedback (IFF) proposed by Ref. [19], resonant control from Refs. [20,21], and the regenerative damping systems in which dissipated energy is reutilized for actuation presented in Refs. [22,23]. However, for most systems and for high gain values, DVF can lead to instabilities, compromising the stability of the system. Methods can be found to improve the stability of the DVF: the placement of pairs of poles and zeros in the open-loop transfer function [24,25], a compensator in the feedback loop [26], compensator filters to counterbalance the phase lag [27], and inerters to increase the apparent mass [28].

With hybrid mass dampers (HMD) the idea is to combine active systems with an optimal passive device. The objective is threefold: (1) improve performance, (2) reduce power consumption, and

¹Corresponding author.

Contributed by the Technical Committee on Vibration and Sound of ASME for publication in the JOURNAL OF VIBRATION AND ACOUSTICS. Manuscript received August 23, 2021; final manuscript received January 3, 2022; published online January 31, 2022. Assoc. Editor: Ryan L Harné.

(3) ensure fail-safe behavior, i.e., the damper will work as a tuned mass damper when the controller is turned off [29]. Systems have been proposed such as an HMD with H_{∞} optimum parameters to minimize both response and control effort [30], a fail-safe system [31], a dual loop approach to increase stability margins [32], an FXLMS controller with a resonant isolation system (SARIB) for helicopter applications [33], delay resonators [34], a tunable vibration absorber [35], an adaptive inertial mass device [36], and an hyperstable HMD [25,37].

Active systems need a power supply to feed the actuator. The analysis of the power flow delivered by this external source provides an indication of the stability and performance of the control device, as shown in Refs. [38,39]. These observations are essential for understanding the stability of the devices, especially when the dynamics of the actuator can modify the phase between the command and the resulting control force, as in the case of an inertial actuator [39,40].

SISO based on a simple input of the supporting structure (unlike many more complex control laws such as the dual loop control law [29]).

In this paper, a focus is done on HMD which combines passive damping and active vibration control which is based on a SISO system with a single input from the primary mass (unlike many more complex control laws such as the dual loop control law [29]). The analysis is carried out in terms of power flow and the interpretation of the hybrid device in term of equivalent mechanical system. The proposed hybrid system controller is fail-safe but also unconditionally stable in theory [25]. Numerical simulations based on an experimental model illustrate the system's performance. The experimental validation is performed with the Hybrid-TSAR, developed and patented by Airbus Helicopter and INSA-Lyon [41]. The first part is dedicated to the theory with a power flow analysis carried out on an inertial damper and an extension to HMD and the α -HMD. The second part is devoted to the experimental validation via performance and power flow with both excitation from the bottom in the frequency domain and shock response in the time domain.

2 Theory and Working Principle

2.1 Power Flow Analysis on An Inertial Damper. One of the main issues of active and hybrid systems is to understand the power flows between the device and the main host structure because it gives information on stability properties and the power supply needed. In order to understand these flows, an isolated Active Mass Damper is analyzed. The device is illustrated in Fig. 1, the dynamics of the host structure is not modeled, in order to decouple the possible interactions in this first analysis.

In Fig. 1, a feedback loop representing the active part of the device can be observed. The sensor is a velocity sensor ($\dot{x}_1 = V_1$), and the actuator generating the control force F_a , is ideal. It acts between the host structure (here the ground) and the mobile mass of the damper (m_{abs}). The mobility of the device is written in the Fourier domain as:

$$Y(j\omega) = \frac{V_1(j\omega)}{F_1(j\omega)} = \frac{-\omega^2 m_{abs} + j\omega c_{abs} + k_{abs}}{-\omega^2 m_{abs}(H(j\omega) + c_{abs} + k_{abs}/(j\omega))} \quad (1)$$

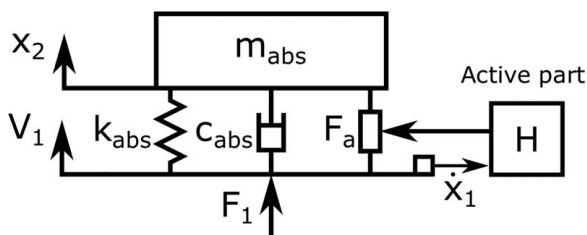


Fig. 1 Implementation of active damping using DVF

where $V_1(j\omega)$ and $F_1(j\omega)$ are the velocity and the force, respectively, of the host structure, m_{abs} , c_{abs} , and k_{abs} are the mass, the damping, and the stiffness of the damper, respectively, ω is the pulsation and $H(j\omega)$ is the control law.

In the case of a passive device, the control law $H(j\omega)$ is set to zero. Usual AMD uses a control law known as DVF where $H(j\omega)$ is a simple gain. Depending on the dynamics of the host structure and the damper this control law can be very efficient but is never unconditionally stable. These stability limits are well known. The resulting active power can be computed by

$$P_a(j\omega) = \frac{1}{2} V_1^*(j\omega) \text{Re}(Y(j\omega)^{-1}) V_1(j\omega) \quad (2)$$

where $V_1^*(j\omega)$ and $Y(j\omega)^{-1}$ are, respectively, the complex conjugate of the velocity and the impedance: the inverse of mobility of the host structure.

Basically, the device is considered as hyperstable if this quantity is always positive. That means that the device only absorbs and dissipates energy from the host structure in the same way as a purely passive system does.

In the first calculus, for the sake of simplicity, a perturbation is considered as an imposed displacement of the ground. Then, the input of the system is the velocity V_1 , a white noise with constant power spectral density. This results in a weak coupling in which the AMD does not modify the dynamics of its host structure. Nevertheless, it provides clear understanding of the power flows at the interface. The parameters of the system are $m_{abs} = k_{abs} = 1$ and $c_{abs} = 0.02$ ($\xi_{abs} = c_{abs}/\sqrt{k_{abs}m_{abs}} = 1\%$).

The resulting active power for a passive damper (deep blue curve) and a classical AMD using DVF (dotted black curve) are shown in Fig. 2. Both active systems have a gain loop of $g = 2000$.

It can be seen that the active power of the passive damper is always positive, which means that the system is purely dissipative. It can also be seen that the active power linked to the AMD using the DVF law is not always positive. Under its resonance frequency its active power drops; that means that the device delivers energy to the host system. These curves depict the well-known stability problem under the resonance frequency of the resonant device. This is the reason why commercial AMDs have very low frequencies compared to the frequencies of the host structures that they equip.

A specific control law $H(j\omega)$ can be designed to modify the resulting power flow. Again considering that V_1 is a white noise with normal power spectral density and without damping ($c_{abs} = 0$), conditions are found on $H(j\omega)$ in order to obtain $P_a > 0$.

The active power can be written as

$$P_a(\omega) = \frac{1}{2} \text{Re}(Y(j\omega)^{-1}) \quad (3)$$

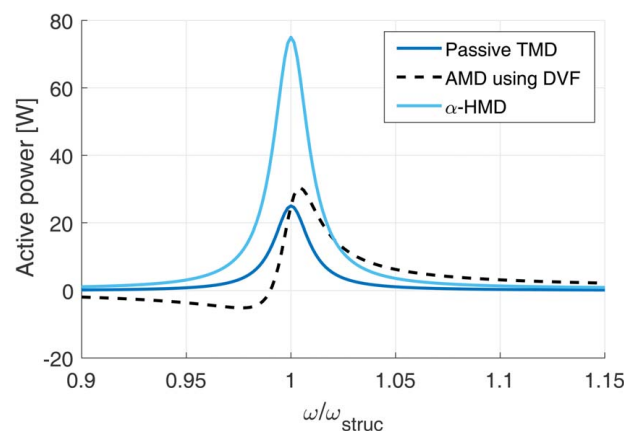


Fig. 2 Active power comparison among passive TMD, AMD using DVF and α -HMD (Color version online.)

using the mobility expression,

$$P_a(\omega) = \frac{1}{2} \operatorname{Re} \left(\frac{-\omega^2 m_{abs} (H(j\omega) + k_{abs}/(j\omega))}{-\omega^2 m_{abs} + k_{abs}} \right) \quad (4)$$

after several steps,

$$P_a(\omega) = \frac{-\omega^2 \operatorname{Re}[H(j\omega)]}{2m_{abs}(\omega_{abs}^2 - \omega^2)} \quad (5)$$

to ensure stability, the active power has to be positive ($P_a > 0$). Thus, the resulting two conditions depend on the pulsation (ω):

- for $\omega < \omega_{abs}$, the real part of the control has to be negative ($\operatorname{Re}[H(j\omega)] < 0$)
- for $\omega > \omega_{abs}$, the real part of the control has to be positive ($\operatorname{Re}[H(j\omega)] > 0$)

These conditions result in a phase shift of the control law around the resonance frequency of the control device. A simple way to achieve these conditions is to build the control law as follows:

$$H(j\omega) = g \left(\frac{j\omega + \omega_{abs}}{j\omega} \right)^2 \quad (6)$$

where g is the gain of the control loop.

The active power using this modified direct velocity feedback is plotted in Fig. 2 in light blue. It can be clearly seen that the active power is now positive over the whole frequency range. The hybrid mass damper is now theoretically hyperstable. That means that whatever the gain (g) of the control loop, the device always absorbs energy from the host structure.

2.2 Extension to Hybrid Tuned Mass Damper. As described in the introduction, the use of a Tuned Mass Damper coupled with an active loop can present several advantages (fail-safe behavior, low consumption, etc.). The aim of this part is to extend the previous analysis of power flow to hybrid systems based on a TMD. The dynamics of the host structure must now be considered to understand the interaction with the tuned damper. The structure to be controlled and the hybrid damper are illustrated in Fig. 3. The TMD is designed according to the Den'Hartog criteria.

Passivity formalism can be used to understand the hyperstable behavior of the device. The passivity theory is a convenient way of interpreting and representing Lyapunov-like functions [42], as Lyapunov functions can be considered as a generalization of the notion of energy in dynamic systems. Passivity theory formalizes the use of these functions to describe and analyze the energy flow in subsystems.

The dynamics of a physical system satisfies the energy conservation principle: the variation of stored energy is the sum of external

power input and internal power generation. This concept can be written for a system i [42]:

$$\dot{V}_i(t) = y_i^T \cdot u_i - G_i(t) \quad (7)$$

with V_i is the scalar function representing the stored energy in subsystem i , G_i is the scalar function representing the internal power generation (V_i and G_i are scalar functions in SISO case), y_i vector of the outputs, and u_i vector of the inputs.

In our case, for the sake of simplicity, without internal mechanical damping ($c_{struc} = c_{abs} = 0$), the internal power generation mechanisms are linked only to the power flow generated by the actuator driven by the controller and its control law $H(j\omega)$. Considering a perfect sensor and actuator and velocity feedback, the G function can be written in the Fourier domain as:

$$G(j\omega) = -F_a(\dot{X}_{abs} - \dot{X}_{struc}) \quad (8)$$

and then

$$G(j\omega) = (\dot{X}_{struc})^2 H(1 - \dot{X}_{abs}/\dot{X}_{struc}) \quad (9)$$

As explained previously, the resulting system is considered passive if:

$$\operatorname{Re}[G(j\omega)] > 0 \quad (10)$$

This passivity behavior means that the system is purely dissipative. Once again, H can be tailored to interact with the dynamics of the structure to ensure hyperstability. This condition allows to adopt the same design of H as in the previous section. The sign of H has to change depending on the sign of the transmissibility function, which obviously depends on the tuning frequency of the absorber.

To illustrate this unconditional stability, Fig. 4 show the open loop transfer functions (Bode and Nyquist) for a usual DVF (in blue) and a modified DVF (alpha controller in red).

Depending on the loop gain stability is not guaranteed for a classical DVF. This instability can be clearly identified in Fig. 4 blue curves), where the phase of the open-loop transfer function rises above 180 deg at low frequency and where the Nyquist diagram passes to the left of the -1 point.

Regarding the control law proposed, it can be interpreted as a phase compensator. The phase of the resulting control law is illustrated in Fig. 4(a). This phase compensator results in an open loop transfer function satisfying the condition of Eq. (10), where the active power must be positive to ensure stability. The open loop transfer function plotted in red in Fig. 4(a) illustrates the final stability. Moreover, on the Nyquist diagram (Fig. 4(b)), the -1 point is now on the left whatever the gain of the control loop.

These considerations were established with the simplification of a null damping ($c_{struc} = c_{abs} = 0$). In practice, the tuning of the alpha parameter does not have to be very accurate. With a non-zero damping, another source of dissipation exists and the condition on the phase of the controller law written in Eq. (10) is not perfectly verified. It can be shown using the Routh-Hurwitz criterion that the stability condition on parameter α is

$$\omega_1 < \alpha < \omega_2 \quad (11)$$

where ω_1 and ω_2 are the two eigenfrequencies of the coupled system (HMD + host structure) and where α is the frequency when $\phi_{H(j\omega)} = -90$ deg. The frequency range $[\omega_1, \omega_2]$ depends on c_{abs} and c_{struc} .

Figure 5 shows the template of the phase of the controller to ensure hyperstability.

2.3 The α -Hybrid Mass Damper. The authors have already shown in Refs. [25,37] that applying direct velocity feedback on a TMD is not a viable solution in terms of stability. Sections 2.1 and 2.2 show that the phase must be modified. Consequently, in

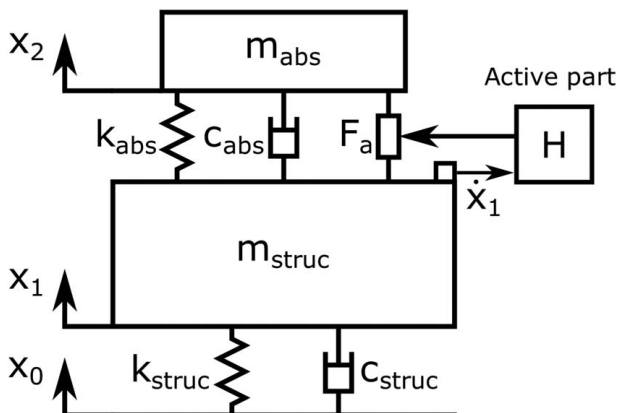


Fig. 3 Diagram of the hybrid damper on the primary structure

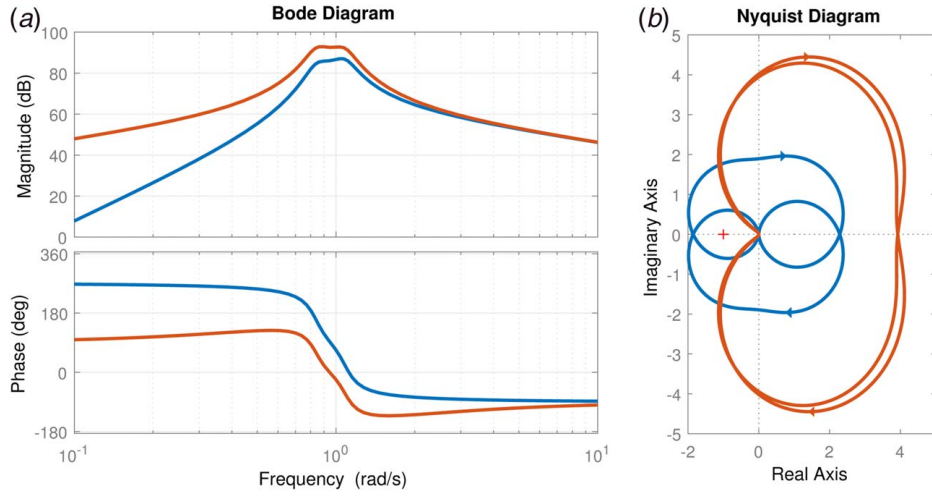


Fig. 4 Comparison of open loop gain between usual DVF and α -controller: (a) bode diagram and (b) Nyquist diagram (Color version online.)

previous sections, the so called α -controller was introduced to ensure stability and performance. It can be written as follows:

$$H_\alpha(j\omega) = g \left(\frac{j\omega + \alpha}{j\omega} \right)^2 \quad (12)$$

where α is tuned on the resonance frequency of the device (ω_{struc}) to ensure the hyperstability of the system g is the gain.

Figure 6 shows the resulting transmissibility function. A comparison is made between the passive tuned mass damper (dark blue curve) and the α -HMD with a gain (g) equal to 2000 (light blue curve). Stability is guaranteed due to the phase compensation in the open-loop transfer function (Fig. 4(a)). The previous parts focused on stability, whereas Fig. 6 quantifies the performance. As expected, the transmissibility amplitude is drastically reduced in the vicinity of ω_{struc} . More theoretical and simulation analyses can be found in Refs. [25,37].

The power that flows from the structure is calculated using the formula below:

$$P = F_a^* V_{rel} + c_{abs} V_{rel}^2 + k_{abs} x_{rel} V_{rel} \quad (13)$$

where F_a is the active force, x_{rel} is the relative displacement, and V_{rel} is the relative velocity. The active power (P_a) is the real part of the power:

$$P_a = \text{Re}(P) = \text{Re}(F_a^* V_{rel} + c_{abs} V_{rel}^2 + k_{abs} x_{rel} V_{rel}) \quad (14)$$

The active power of a spring is null, so the total active power which flows from the structure can be written as follows:

$$P_a = \text{Re}(F_a^* V_{rel} + c_{abs} V_{rel}^2) \quad (15)$$

Figure 7(a) shows the numerical active power which flows for passive TMD and for hybrid-TMD (HMD) using the α -controller

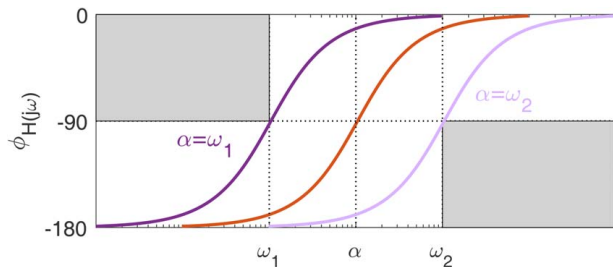


Fig. 5 Phase profile limits of the control law to ensure hyperstability

with the gain g equal to 1000 and 2000. As expected, pole spreading is observed when the gain increases, illustrating the virtual addition of mass. Only a few modifications of the active power at the resonance frequency of the primary structure are observed. In the frequency domain, the active power is always positive ($\text{Re}(P) > 0$) which means stability is ensured. Figure 7(b) shows the numerical cumulative sum of the active power flows for passive TMD and for hybrid-TMD (HMD) using the α -controller with the gain g equal to 1000 and 2000. The numerical cumulative sum of the active power flows for passive TMD is eight times greater than for the passive TMD.

2.4 Mechanical Analogy. One interesting way to understand the hyperstability properties and the dynamical behavior of the proposed controller is to find an equivalent mechanical model. In this part, for sake of simplicity, the mechanical damping of the absorber is omitted. The resulting hybrid device is represented in Fig. 8(a).

Considering $F_a(j\omega) = H(j\omega) \times V_1(j\omega)$, one can write the resulting impedance Z_H of the hybrid device, in Fourier domain:

$$Z_H(j\omega) = \frac{F_1(j\omega)}{V_1(j\omega)} = \frac{j\omega m_{abs} k_{abs}}{k_{abs} - \omega^2 m_{abs}} + \frac{-\omega^2 m_{abs}}{k_{abs} - \omega^2 m_{abs}} H(j\omega) = Z_{TMD}(j\omega) + Z_a(j\omega) \quad (16)$$

where Z_{TMD} is the impedance of a passive TMD and Z_a represents the active part. The two systems can be considered as acting in parallel.

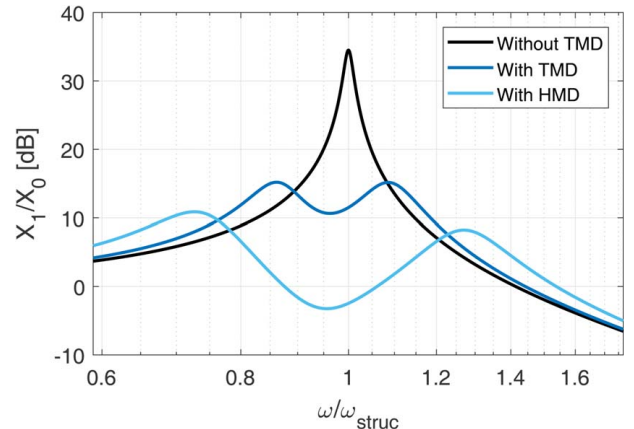


Fig. 6 Transmissibility functions x_1/x_0 without TMD, for passive TMD and for hybrid-TMD using the proposed controller

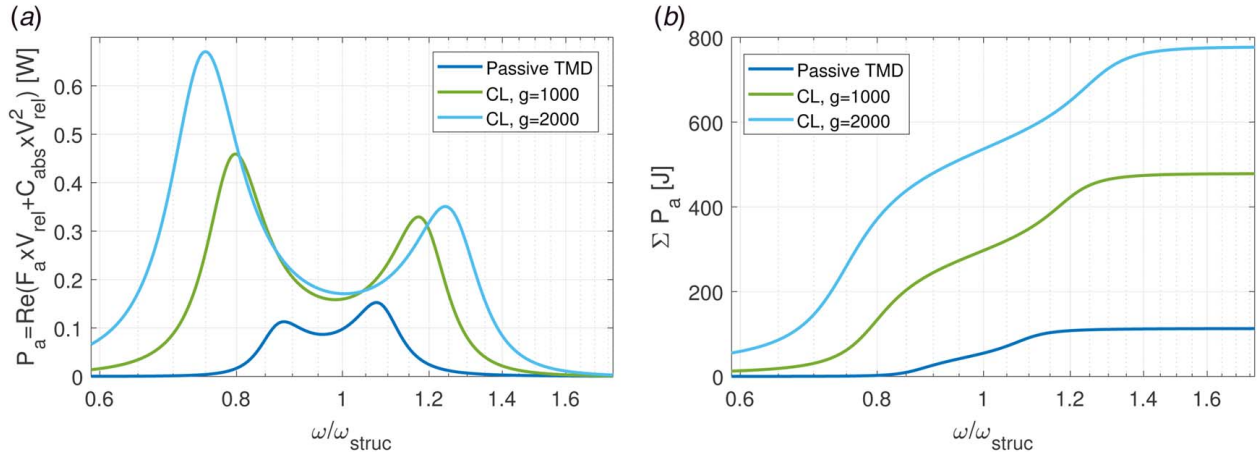


Fig. 7 (a) Numerical active power and (b) numerical cumulative sum of the active power

For the active part, by applying the α -controller law, with $\alpha = \omega_{abs}$, then $H(j\omega) = g((j\omega + \omega_{abs})/j\omega)^2$, one can find:

$$Z_a(j\omega) = \frac{-\omega^2 m_{abs}}{k_{abs} - \omega^2 m_{abs}} H(j\omega) = \frac{-g\omega^2 + 2g\omega_{abs}j\omega + \omega_{abs}^2 g}{\omega_{abs}^2 - \omega^2} \quad (17)$$

An equivalent mechanical system having the same impedance can be found as shown below.

On the other side, the system illustrated in Fig. 8(b) represents a passive TMD, associated with a sky hook damper c_{eq} and an inertia m_{eq} in series with a spring k_{eq} . Let's remind that an inerter is a device which generates a force proportional to relative accelerations between its two connections. One can find its equivalent mechanical impedance Z_{eq} that can be written:

$$Z_{eq} = Z_{TMD} + c_{eq} + \frac{1}{\frac{j\omega}{k_{eq}} + \frac{1}{j\omega m_{eq}}} \quad (18)$$

with $\omega_{eq}^2 = k_{eq}/m_{eq}$, Eq. (18) can be written as follows:

$$Z_{eq} = Z_{TMD} + \frac{-c_{eq}\omega^2 + k_{eq}j\omega + \omega_{eq}^2 c_{eq}}{\omega_{eq}^2 - \omega^2} \quad (19)$$

By identification with Eq. (17), considering $\alpha = \omega_{abs}$, the mechanical parameters of the analogy can be found:

$$k_{eq} = 2g\alpha, \quad m_{eq} = \frac{2g}{\alpha}, \quad c_{eq} = g \quad (20)$$

In conclusion, the proposed control law increases the equivalent mass of the absorber in proportion to the gain of the control loop, while keeping its tuning constant. In addition, it adds in parallel a skyhook damper whose damping is equal to the gain.

One can note that the existence of a full mechanical analogy prove again the stability of the active system. Thus, the hyperstability property is guaranteed given idealized sensors and actuators are employed.

3 Experimental Validation

3.1 Setup and Transducer. The experimental setup is a two-degrees-of-freedom system, one linked to the main structure which has to be controlled, and one linked to the absorber. The main structure ($m_{struc} = 153.4$ kg) is designed to behave like a single-degree-of-freedom (x_1) which is suspended by flexible blades. High stiffness is ensured by these blades working in flexion. Its resonance frequency is experimentally tuned to be around 17 Hz, by testing various blades with different widths. Finally, the resulting stiffness of the primary structure k_{struc} is equal to 1745.1 kN/m. The blades are made of blue steel in order to resist high strain.

The HMD presented is based on the Hybrid-TSAR, developed and patented by Airbus Helicopter and INSA-Lyon [41]. Basically, it consists of a one mechanical degree-of-freedom system (x_2) designed as a TMD. The moving mass is guided by two sets of flexible membranes that guarantee the resulting stiffness. Two magnets are fixed at the extremities of the moving mass, contributing to the total mass of the moving part. Each magnet is surrounded by a coil. One voice-coil system is dedicated to the passive behavior, dissipating energy through a tunable load, and the second one represents the active part.

The two-degree-of-freedom system is mounted on the 6-axis shaker of the Equipex PHARE (Fig. 9). This unique test facility in the national public research facility has large capacities and can generate vibrations on six axis. The excitation from the bottom is provided by the six-axis shaker though only the x -axis is used for this application (x_0). The optimal TMD's parameters are experimentally identified ($m_{abs} = 9.6$ kg, $k_{abs} = 96.7$ kN/m, and $\xi_{abs} = 10.6\%$), and the resonance frequency of the absorber is around 16 Hz. Since its mechanical damping is very weak (around 1%), damping is provided by the coil-magnet combination coupled with a tunable resistor ($R1$). The active part (second voice-coil system) is driven by a current amplifier (Kepco BOP 72-6M). Another set of tuning parameters (a different ω_{abs}) was studied in a previous publication [29] to validate a fail-safe dual-loop controller. The experimental setup is consistent with the two degrees-of-freedom illustrated in Fig. 3.

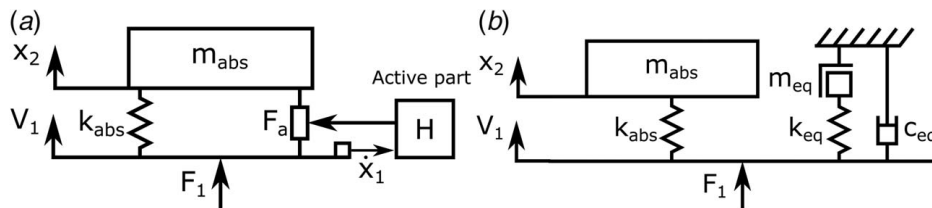


Fig. 8 (a) Schematic of the hybrid device and (b) its equivalent mechanical model

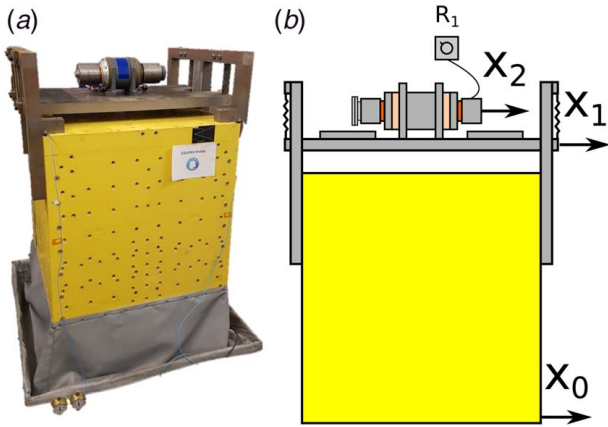


Fig. 9 (a) Six-axis shaker of the Equipex Phare with the whole system mounted on it and (b) diagram of the system

For the applications intended, the frequency aspects are discussed (Sec. 3.3), and the concepts related to the shock response in the time domain time response are studied (Sec. 3.4).

3.2 Practical Considerations. The control law is a modified velocity feedback with a phase compensator where α is tuned on the resonance frequency of the device (ω_{struc}) to ensure the hyperstability of the system. This hyperstability property can also be observed on the root locus (Fig. 10, gray curves). Whatever the loop gain, the poles are still on the left side of the root locus. Theoretically, an infinite gain margin is ensured. Pole spreading is observed when the gain increases as expected in Fig. 6. In practice, a low frequency drift of the feedback instruction is observed due to the double integration. Therefore, a Chebyshev type I (order 4) high pass filter is used. The yellow curves on Fig. 10 show the practical root locus where the Chebyshev filterpole is observed (Fig. 10(b)). The root locus obtained from the experimental model shows that hyperstability is lost. A short part of the root locus goes to the right half plan but it corresponds to very high gain behavior (50 times higher than the chosen gain of 2000).

The stability margins are still very high, but they do not represent a limit to the performance. Other limits due to the stroke displacement of the absorber and the saturation of the amplifier will be more restrictive than this stability limit.

3.3 Excitation From the Bottom – Frequency Analysis

3.3.1 Vibration Attenuation. The excitation from the bottom is provided by the six-axis shaker but only the x -axis is used for this application. Six hydraulic cylinders work together to ensure correct enslaving in the x direction, driven in displacement. Keeping the five other directions slaved to 0. A swept sine is applied by the shaker between 5 and 30 Hz ($x_0 = 0.05 \times 10^{-3} \times \cos(\omega t)$ [m]). Three configurations are tested without TMD, with passive TMD and with the HMD Hybrid-TSAR. The last configuration used the α -controller in closed loop with several control gains g . The speed of the main structure (\dot{x}_1) is obtained by integrating the signal of an accelerometer placed on it.

Figure 11(a) shows the experimental transmissibility functions x_1/x_0 without TMD, for passive TMD and for hybrid-TMD (HMD) using the α -controller with the gain g equal to 1000, 2000, and 2500. At 17 Hz, the resonance of the primary structure, the transmissibility amplitude is drastically reduced from 23 dB for the passive TMD until 37 dB for the higher control gain. In the best configuration ($g = 2500$), the actively added mass, predicted by mechanical analogy, is about 46 kg. This results in a total mass 5.8 times greater than the initial mass of the absorber. It appears consistent with the observation of pole spreading (as also predicted by the root locus). What is notable is that transmissibility is less than 0 dB, meaning that the amplitude of x_1 is smaller than that of x_0 .

The active force is proportional to the current delivered by the amplifier. In Fig. 11, when the gain is equal to 2500, the second mode around 22 Hz was impacted, and the saturation of the current amplifier was observed. The control current driving the HMD was up to ± 6 A. This is not a stability problem and the main limitation is practical.

Numerical simulations were performed and good agreement with the experimental data is observed (Fig. 11(b)).

It could be interesting for civil engineering for example to evaluate the cumulative sum of the transmissibility. This indicator

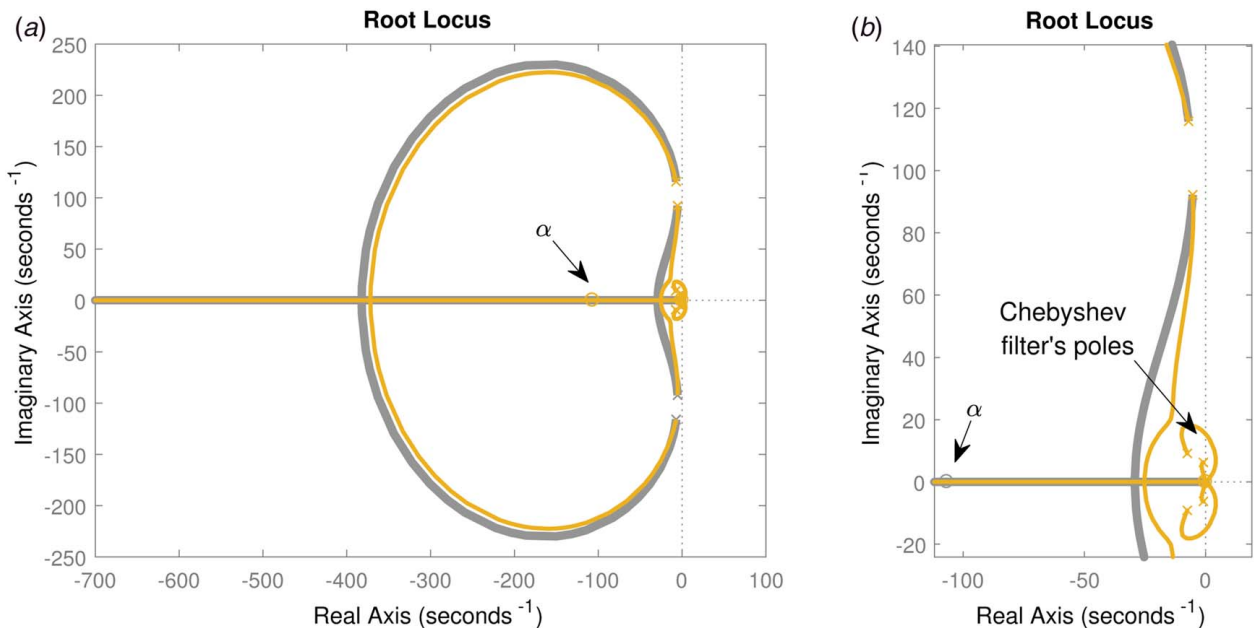


Fig. 10 (a) Theoretical root locus with the α -controller in gray. Practical root locus including the Chebyshev type-I filter in yellow and (b) zoom on the root locus.

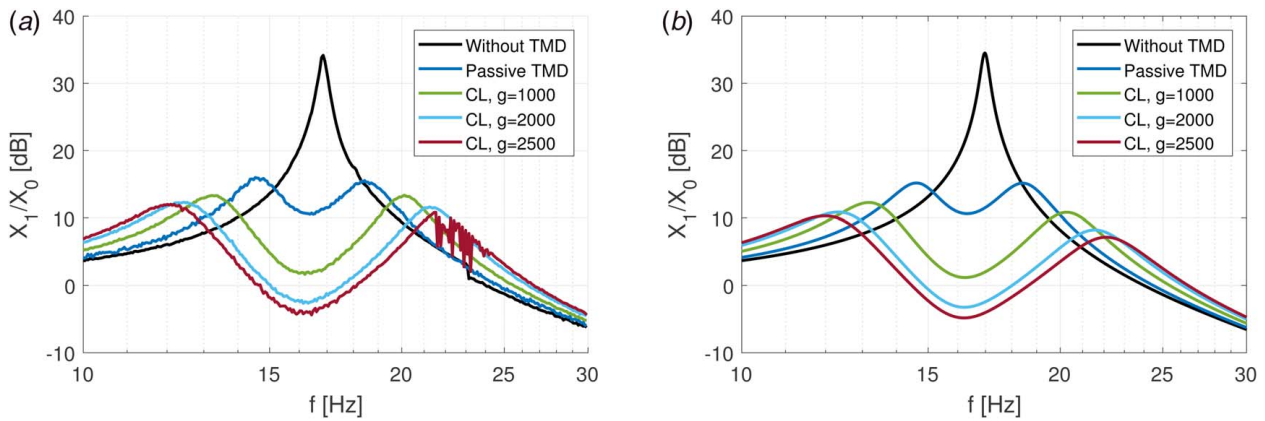


Fig. 11 Transmissibility functions x_1/x_0 without TMD, for passive TMD and for hybrid-TMD using the α -controller at different gains g : (a) Experimental results and (b) numerical simulations

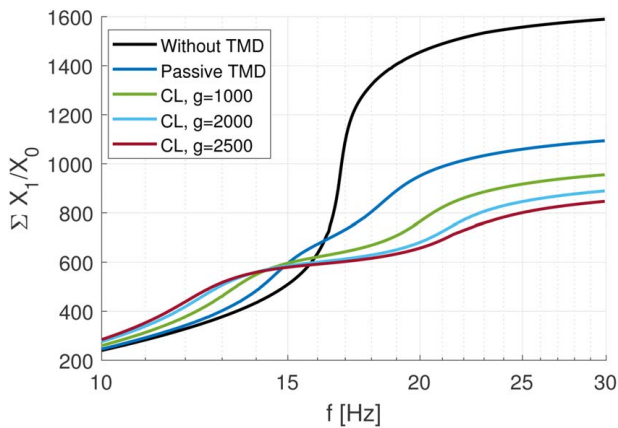


Fig. 12 Experimental cumulative sum of the transmissibility functions x_1/x_0 without TMD, for passive TMD and for hybrid-TMD using the α -controller at different gains g

shows the wideband effect and can be generally related to the fatigue of the materials. Figure 12 shows the cumulative sum of the transmissibility functions x_1/x_0 for passive TMD and hybrid-TMD using the α -controller at different gains g . The performances of the different configurations are compared over the frequency range of interest. With the best configuration ($g = 2500$), the cumulative sum of the transmissibility is divided by two compared to the configuration without absorber.

For applications where the perturbation is harmonic, the reduction of transmissibility can be observed on the time domain at 17

Hz (Fig. 13(a)). The amplitude is divided by 14 for the passive TMD until 70 for the higher control gain. Figure 13(b) shows a zoom to show the amplitude of the response for the passive and hybrid systems.

3.3.2 Power Flow Measurement. The power flowing from the structure is calculated using the same formula (Eq. (13)) as in Sec. 2.3.

The power is a complex quantity; it is necessary to consider the active part and the reactive part of the power to conclude on the hyperstability of the system. Figure 14(a) shows the experimental active power which is the real part of the total power. In the frequency domain, it can be observed that the active power is always positive ($\text{Re}(P) > 0$). The system is proved experimentally to be purely dissipative.

Figure 14(b) shows the experimental cumulative sum of the active power. As shown in the numerical part (Sec. 2.3, Fig. 7), the same trend is observed experimentally. Pole spreading is observed when the gain increases and the experimental cumulative sum of the active power flowing at the interface for the hybrid TMD is greater than that of the passive TMD (six times).

3.4 Shock Response – Time Analysis

3.4.1 Vibration Attenuation. This part focuses on the transient response of such a system. Shocks were injected using a light pendulum system with direct impact on the mass $m_{struc}(x_1)$. Very high repeatability was observed. Consequently, the next figures illustrate the behavior of the system for one representative impact.

Figure 15 shows the acceleration response to an impact with a passive TMD and with a hybrid one. It can be seen that the acceleration is globally reduced, especially at the beginning (cf. zoom)

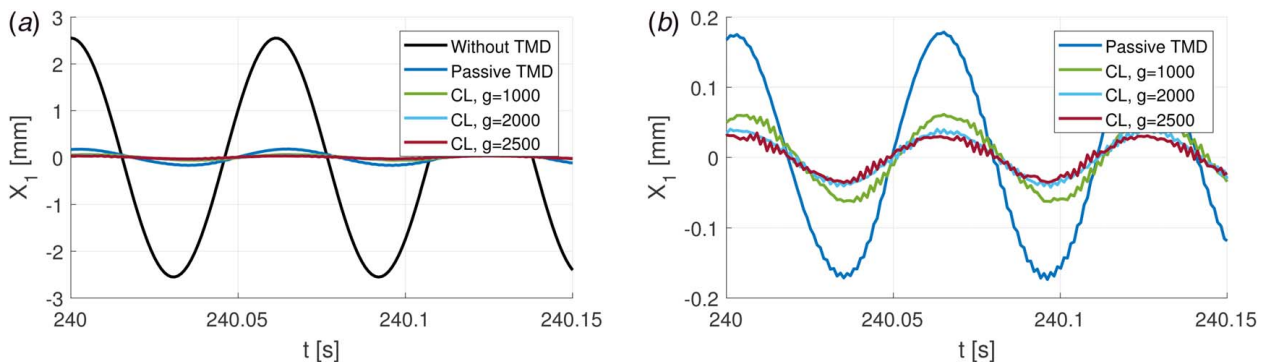


Fig. 13 (a) Experimental displacements versus time at 17 Hz for the passive TMD and the hybrid-TMD using the α -controller at different gains g and (b) zoom

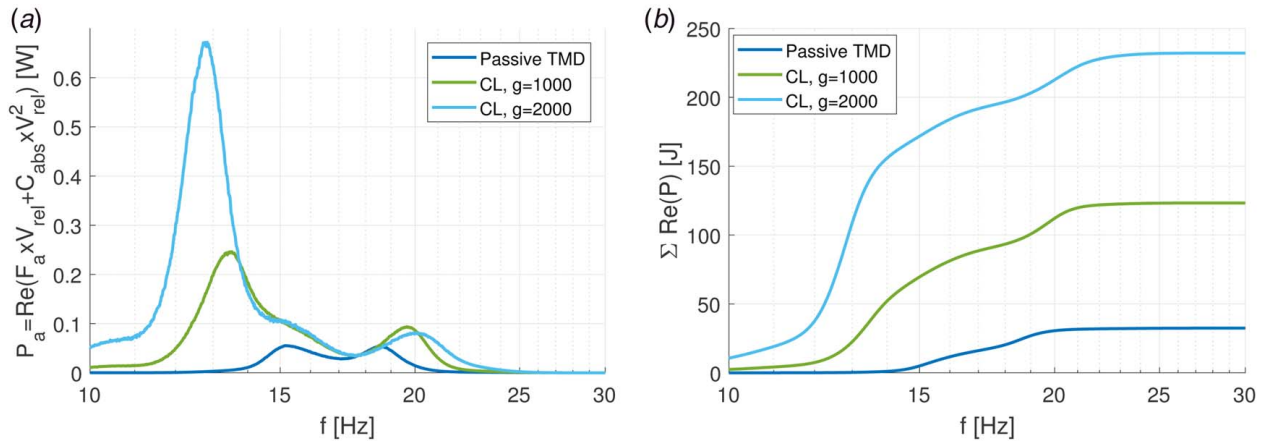


Fig. 14 (a) Experimental active power and (b) experimental cumulative sum of the active power

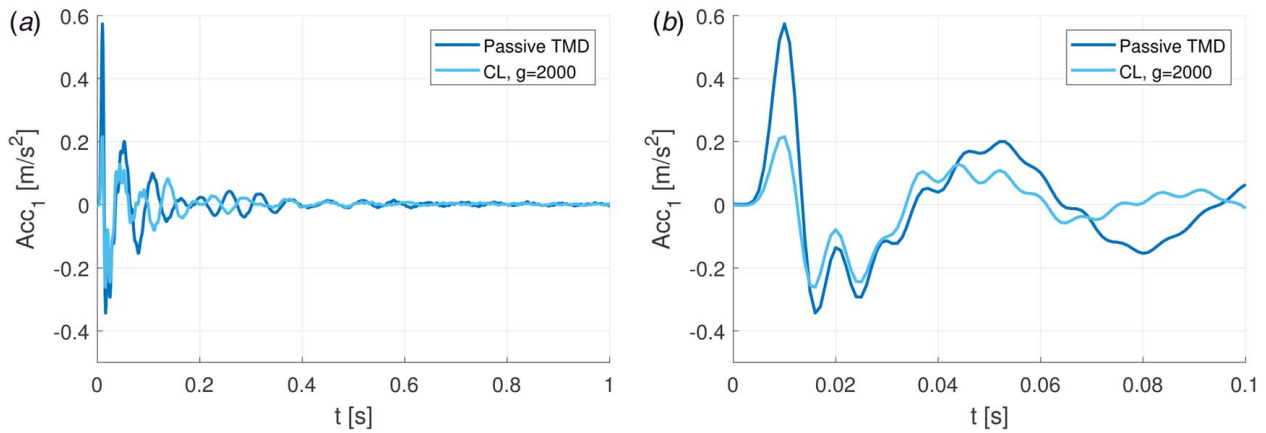


Fig. 15 Measured acceleration of mass m_{struct} , without and with the α -controller: (a) global view and (b) zoom

where the maximum acceleration is reduced by a factor 3. Indeed, passive TMDs are known to have poor ability to reduce the first period of vibration or globally transient perturbation. This can be understood by looking the relative velocity of the absorber ($\dot{x}_2 - \dot{x}_1$) shown in Fig. 16.

Figure 16 presents experimental relative velocity signals between the moving mass of the hybrid tuned mass damper and the displacement of the mass m_1 without and with control (closed loop). One

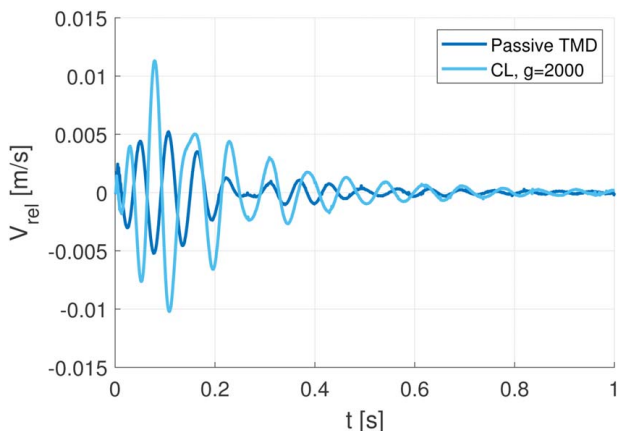


Fig. 16 Relative velocity under impulse excitation

can clearly see the slow increase of the oscillation amplitude for the passive device. The hybrid one reacts much faster and with higher amplitudes, therefore dissipating energy and counteracting the vibrations. This is mainly due to the active force illustrated in Fig. 17. Hybrid systems combine two behaviors that can be summarized as follows:

- Passive behavior: HMD has higher relative amplified stroke displacement than usual TMD, dissipating more energy.
- Active behavior: HMD acts as an AMD, the applied force is opposed to the velocity of the main structure in order to absorb energy.

In practice, depending on the transducer and the control law, active force can introduce energy into the host structure. The experimental power flow estimation is presented in Sec. 3.4.2.

3.4.2 Power Flow Estimation. Figure 18 shows the power dissipated in the passive part, which is positive. This part is directly quantifiable because the setup allows the measurement of the relative velocity between the host structure and the absorber (measured via the voltage at the passive voice-coil terminals). This part of the power, proportional to the square root of the relative velocity (Fig. 16) is greater for the HMD than for the passive TMD. It results in a higher amount of energy electrically dissipated through the load associated with the passive part for the HMD.

Figure 19 shows the total power of the active part of HMD. Although it is mainly positive (meaning dissipation), it can be seen that it can be negative. In practice the sign of the power

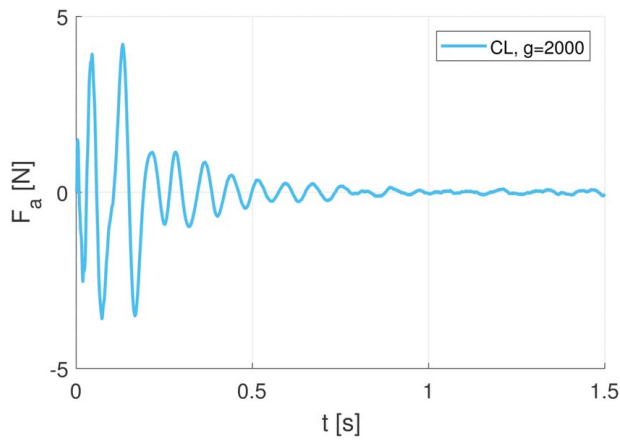


Fig. 17 Active force under impulse excitation

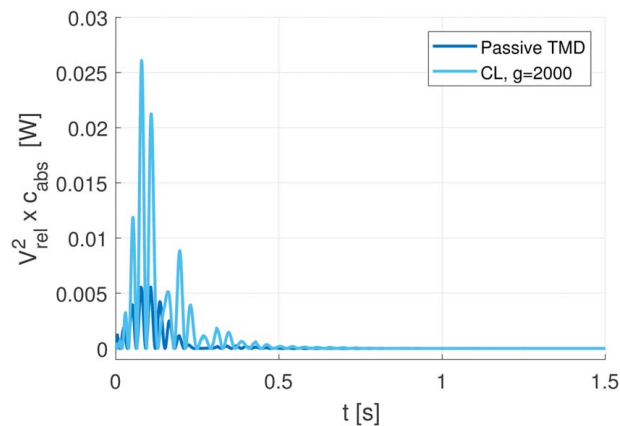


Fig. 18 Dissipated power in the passive part

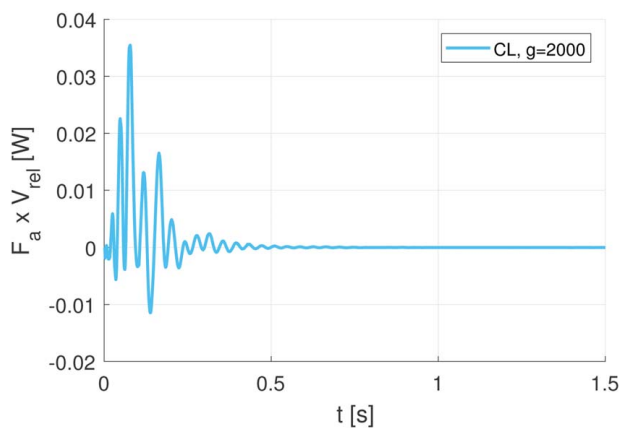


Fig. 19 Instantaneous total power of the active part of the HMD

seems too restrictive to conclude on the hyperstability property. The quantities plotted concern the active part and the reactive part of the power which cannot be separated in a transient signal with the setup proposed.

The cumulative sum of the total power which flows at the interface is shown in Fig. 20. For the HMD, the slope is mostly positive except around $t=0.2$ s, the power is mainly absorbed. The total power is 6 times greater after 1 s for the HMD than for the passive TMD.

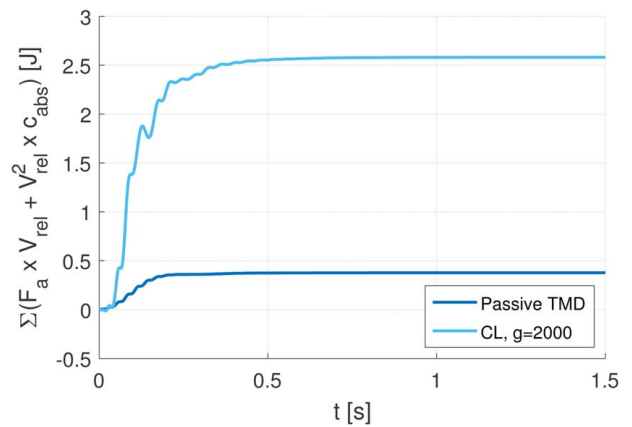


Fig. 20 Cumulative sum of the total power flowing at the interface

4 Conclusion

This paper presented an original analysis and experimentation for a HMD which combines an active system with an optimal passive device. The approach is based on the power flow analysis and the equivalent mechanical system of the hybrid device. The control law is a modified velocity feedback with a phase compensator. The α -controller is hyperstable and ensures fail-safe behavior. A comparison was made between the passive tuned mass damper and the α -HMD with control in terms of the transmissibility function. The amplitude was drastically reduced at the vicinity of ω_{struct} . The numerical model was fed with experimentally identified parameters. The theoretical analysis of the power flow showed that the system is purely dissipative, meaning hyperstable, as illustrated through the full mechanical analogy. Hybrid device can be seen as an association of an inerter, a spring and a skyhook damper. It results that the gain of the control loop increases the equivalent mass and damping of the absorber. The experimental validation was performed with a two-degrees-of-freedom system. The main structure was excited in one direction with the six-axis shaker of the Equipex PHARE. The design of the HMD [41] was based on an optimal TMD integrating a co-located pair of voice-coil devices. One was dedicated to the passive behavior of the TMD, the other one was used as an actuator. Good agreement was observed between the experimental transmissibility function and the numerical one. Analysis in the frequency domain clearly showed that the active power was positive, highlighting that the system is purely dissipative. In the time domain subject to shock, this notion appeared more difficult to analyze. Nevertheless, the hybrid device reacted much faster and with higher amplitudes than the passive one. In this case, a global indicator was used: the cumulative sum of the power showed the increase in absorbed energy versus the passive system. The high strokes of the HMD can be considered as a significant drawback for applications where the available space is limited. In future work and developments, some non-linear behaviors will be introduced. This can be done in the mechanical part to increase the resulting passive force or in the control law itself. Smaller strokes will be expected but also a greater robustness against frequency variations. Of course, these future designs will rise the problem of stability.

Acknowledgment

The authors want to thank the French National Research Agency for the Equipex PHARE (ANR-10-EQPX-43) and F. Legrand (LaMCoS engineer) for his help.

Conflict of Interest

There are no conflicts of interest.

Data Availability Statement

The authors attest that all data for this study are included in the paper.

References

- [1] Aly, A. M., 2014, "Proposed Robust Tuned Mass Damper for Response Mitigation in Buildings Exposed to Multidirectional Wind," *The Structural Design of Tall and Special Buildings*, **23**(9), pp. 664–691.
- [2] Arfiadi, Y., 2017, "Nonlinear Controllers for Active Composite Tuned Mass Dampers," *Procedia Eng.*, **171**, pp. 1178–1185.
- [3] Sakr, T. A., 2017, "Vibration Control of Buildings by Using Partial Floor Loads As Multiple Tuned Mass Dampers," *HBRC J.*, **13**(2), pp. 133–144.
- [4] Salvi, J., Rizzi, E., Rustighi, E., and Ferguson, N. S., 2015, "On the Optimization of a Hybrid Tuned Mass Damper for Impulse Loading," *Smart Mater. Struct.*, **24**(8), p. 085010.
- [5] Xiang, P., and Nishitani, A., 2014, "Optimum Design for More Effective Tuned Mass Damper System and Its Application to Base-Isolated Buildings," *Struct. Control Health Monitor.*, **21**(1), pp. 98–114.
- [6] Den Hartog, J., 1956, *Mechanical Vibrations*, McGraw-Hill Book Company, New York, pp. 122–169.
- [7] Habib, G., Detroux, T., Vigiúé, R., and Kerschen, G., 2015, "Nonlinear Generalization of Den Hartog's Equal-Peak Method," *Mech. Syst. Signal Process.*, **52**, pp. 17–28.
- [8] Asami, T., Nishihara, O., and Baz, A. M., 2002, "Analytical Solutions to H_∞ and H₂ Optimization of Dynamic Vibration Absorbers Attached to Damped Linear Systems," *ASME J. Vib. Acoust.*, **124**(2), pp. 284–295.
- [9] Calafiore, G. C., and Campi, M. C., 2006, "The Scenario Approach to Robust Control Design," *IEEE Trans. Automat. Contr.*, **51**(5), pp. 742–753.
- [10] Soltani, P., Kerschen, G., Tondreau, G., and Deraemaeker, A., 2014, "Piezoelectric Vibration Damping Using Resonant Shunt Circuits: An Exact Solution," *Smart Mater. Struct.*, **23**(12), p. 125014.
- [11] Ali, S. F., and Adhikari, S., 2013, "Energy Harvesting Dynamic Vibration Absorbers," *ASME J. Appl. Mech.*, **80**(4), p. 041004.
- [12] Zhou, D., Hansen, C., and Li, J., 2011, "Suppression of Maglev Vehicle-Girder Self-Excited Vibration Using a Virtual Tuned Mass Damper," *J. Sound Vib.*, **330**(5), pp. 883–901.
- [13] Hagoood, N. W., and von Flotow, A., 1991, "Damping of Structural Vibrations With Piezoelectric Materials and Passive Electrical Networks," *J. Sound Vib.*, **146**(2), pp. 243–268.
- [14] Zhou, S., Jean-Mistral, C., and Chesné, S., 2019, "Electromagnetic Shunt Damping With Negative Impedances: Optimization and Analysis," *J. Sound Vib.*, **445**, pp. 188–203.
- [15] Lu, Z., Chen, X., and Zhou, Y., 2017, "An Equivalent Method for Optimization of Particle Tuned Mass Damper Based on Experimental Parametric Study," *J. Sound Vib.*, **419**, pp. 571–584.
- [16] Preumont, A., and Seto, K., 2008, *Active Control of Structures*, John Wiley & Sons.
- [17] Fanson, J. L., 1987, "An Experimental Investigation of Vibration Suppression in Large Space Structures Using Positive Position Feedback," Ph.D. thesis, California Institute of Technology.
- [18] Goh, C. J., 1983, "Analysis and Control of Quasi Distributed Parameter Systems," Ph.D. thesis, California Institute of Technology.
- [19] Preumont, A., 2002, *Vibration Control of Active Structures: An Introduction*, Vol. 246, Springer.
- [20] Aphale, S. S., Fleming, A. J., and Moheimani, S. R., 2007, "Integral Resonant Control of Collocated Smart Structures," *Smart Mater. Struct.*, **16**(2), p. 439.
- [21] Diaz, I. M., Pereira, E., and Reynolds, P., 2012, "Integral Resonant Control Scheme for Cancelling Human-Induced Vibrations in Light-Weight Pedestrian Structures," *Struct. Control Health Monitor.*, **19**(1), pp. 55–69.
- [22] Fodor, M., and Redfield, R., 1993, "The Variable Linear Transmission for Regenerative Damping in Vehicle Suspension Control," *Veh. Syst. Dyn.*, **22**(1), pp. 1–20.
- [23] Suda, Y., Nakadai, S., and Nakano, K., 1998, "Hybrid Suspension System With Skyhook Control and Energy Regeneration (development of Self-Powered Active Suspension)," *Veh. Syst. Dyn.*, **29**(S1), pp. 619–634.
- [24] Diaz, I., and Reynolds, P., 2009, "Robust Saturated Control of Human-Induced Floor Vibrations Via a Proof-Mass Actuator," *Smart Mater. Struct.*, **18**(12), p. 125024.
- [25] Collette, C., and Chesne, S., 2016, "Robust Hybrid Mass Damper," *J. Sound Vib.*, **375**, pp. 19–27.
- [26] Elliott, S., Rohlfing, J., and Gardonio, P., 2012, "Multifunctional Design of Inertially-Actuated Velocity Feedback Controllers," *J. Acoust. Soc. Am.*, **131**(2), pp. 1150–1157.
- [27] Rohlfing, J., Elliott, S., and Gardonio, P., 2012, "Feedback Compensator for Control Units With Proof-Mass Electrodynamic Actuators," *J. Sound Vib.*, **331**(15), pp. 3437–3450.
- [28] Kras, A., and Gardonio, P., 2017, "Velocity Feedback Control With a Flywheel Proof Mass Actuator," *J. Sound Vib.*, **402**, pp. 31–50.
- [29] Chesné, S., Inquiere, G., Cranga, P., Legrand, F., and Petitjean, B., 2019, "Innovative Hybrid Mass Damper for Dual-Loop Controller," *Mech. Syst. Signal Process.*, **115**, pp. 514–523.
- [30] Cheung, Y., Wong, W., and Cheng, L., 2012, "Design Optimization of a Damped Hybrid Vibration Absorber," *J. Sound Vib.*, **331**(4), pp. 750–766.
- [31] Tso, M., Yuan, J., and Wong, W., 2013, "Design and Experimental Study of a Hybrid Vibration Absorber for Global Vibration Control," *Eng. Struct.*, **56**, pp. 1058–1069.
- [32] Hagedorn, P., and Spelsberg-Korspeter, G., 2014, *Active and Passive Vibration Control of Structures*, Springer.
- [33] Rodriguez, J., Cranga, P., Chesne, S., and Gaudiller, L., 2016, "Hybrid Active Suspension System of a Helicopter Main Gearbox," *J. Vib. Control*, **24**(5), pp. 956–974.
- [34] Olgac, N., and Holm-Hansen, B., 1994, "A Novel Active Vibration Absorption Technique: Delayed Resonator," *J. Sound Vib.*, **176**(1), pp. 93–104.
- [35] Alujević, N., Tomac, I., and Gardonio, P., 2012, "Tuneable Vibration Absorber Using Acceleration and Displacement Feedback," *J. Sound Vib.*, **331**(12), pp. 2713–2728.
- [36] Mayer, D., and Herold, S., 2018, *Passive, Adaptive, Active Vibration Control, and Integrated Approaches*, 04.
- [37] Chesné, S., and Collette, C., 2017, "Experimental Validation of Fail-Safe Hybrid Mass Damper," *J. Vib. Control*, **24**(19), pp. 4395–4406.
- [38] Mahajan, S., and Redfield, R., 1998, "Power Flow in Linear, Active Vibration Isolation Systems," *ASME J. Vib. Acoust.*, **120**(2), pp. 571–578.
- [39] Camperi, S., Tehrani, M. G., and Elliott, S. J., 2018, "Parametric Study on the Optimal Tuning of An Inertial Actuator for Vibration Control of a Plate: Theory and Experiments," *J. Sound Vib.*, **435**, pp. 1–22.
- [40] Camperi, S., Tehrani, M. G., and Elliott, S. J., 2019, "Local Tuning and Power Requirements of a Multi-Input Multi-Output Decentralised Velocity Feedback With Inertial Actuators," *Mech. Syst. Signal Process.*, **117**, pp. 689–708.
- [41] Inquiere, G., Cranga, P., and Chesné, S., 2017, "Resonator, and an Aircraft Fitted With the Resonator," U.S. Patent App. 15/610, 735, Dec. 7.
- [42] Slotine, J. J. E., and Li, W., 1991, *Applied Nonlinear Control*, Vol. 199, Prentice Hall, Englewood Cliffs, NJ.